Journal of Materials Chemistry

Cite this: J. Mater. Chem., 2011, 21, 11323

www.rsc.org/materials

PAPER

Porous graphene oxide frameworks: Synthesis and gas sorption properties†

Gadipelli Srinivas,*[ab] Jacob W. Burress,[a] Jamie Ford[ab] and Taner Yildirim*[ab]

Received 19th April 2011, Accepted 5th June 2011
DOI: 10.1039/c1jm11699a

We report detailed synthesis of a range of porous graphene oxide frameworks (GOFs) by expansion of graphene oxide (GO) sheets with various linear boronic acid pillaring units in a solvothermal reaction. The GOF structures develop through boronate-ester formation as a result of B–O bonding between boronic acids and oxygen functional groups on the GO layers. Synthesized GOFs exhibit periodic layered structures with largely expanded interlayer spacing as characterized by X-ray powder diffraction (XRD). The boronate-ester link formation is further evidenced by Fourier transform infrared (FTIR) and Raman spectroscopy. Furthermore, the strong boronate-ester bonds between GO layers results in improved thermal stability over the precursor GO. The solvent-free, evacuated frameworks provide highly increased accessible surface area for nitrogen adsorption compared to GO alone, which depends on the type and length of the boronic acid, indicating the importance of pillaring unit. Both isosteric heat of adsorption (Q_{st}) and the adsorbed hydrogen capacity per surface area are twice as large as typical porous carbon materials and comparable to metal–organic frameworks (MOFs) with open metal centers. This enhanced Q_{st} and adsorption capacity is attributed to optimum interlayer spacing between graphene planes such that hydrogen molecules interact with both surfaces. Finally, our systematic study reveals the profound effect of both synthesis and activation temperatures to obtain porous framework structures.

1. Introduction

Recently, graphene oxide (GO) based materials have generated tremendous interest for energy related applications because of its multifunctional flexibility.[1–10] The porosity and accessible surface area can be easily tuned for electrochemical/gas storage and catalytic ability by changing the graphene layer spacing or by functionalizing with various chemical groups. Furthermore, the ability to incorporate various functional groups into the interlayer space and the tunable periodic layer structure of GO could possibly help in the design of hybrid porous networks for green energy.[2–6] Modifications of GO layers by targeting the hydroxy and epoxy surface functionalities with both organic and inorganic compounds have been studied previously.[2–14] For instance, the functionality of GO layers was assessed using intercalation or cross-linking with primary aliphatic amines, amino acids, diaminoalkanes and isocyanates.[7–12] GO layers covalently linked with polymers by esterification have also been reported.[3,4,13,14] All these studies reveal only the controllability of the interlayer spacing and hydrophobicity depending on the size and molecular structure of the guests. Despite enormously increased interlayer distance of graphene sheets, the improvements in porosity and surface area are rarely found for gas storage applications.[4,8–14] In one approach, the surface area of graphene sheets was improved to some extent by chemical reduction of GO, but at the same time the interlayer separation was also reduced, thereby reducing the effective molecular adsorption.[15–17] However, given the rich surface functionality of GO layers, it is possible to obtain higher accessible surface areas by keeping GO layers apart using proper choice of pillaring molecular structures.[6,10,18–21] For example, the diisocyanate cross-linked GO hybrids can exhibit BET specific surface areas of 60 $m^2\ g^{-1}$ to 170 $m^2\ g^{-1}$ compared to the $\approx$3 $m^2\ g^{-1}$ for precursor GO. Yet in the case of energy storage applications, one needs to have appreciably higher accessible surface areas.

In the past few years, boronic acids have received tremendous attention as versatile building blocks for the construction of a variety of molecular architectures.[22,23] The interaction between boronic acids and diols has been used recently to form covalent organic frameworks (COFs), a class of porous materials that are metal-free, covalently linked, and highly crystalline.[22,23] In principle, the construction of similar boronic acid-based porous framework materials is possible with GO layers given enough oxy-functional groups. However, a potential problem inherent to the boronic acids is self condensation to form anhydride

[a]NIST Center for Neutron Research, National Institute of Standards and Technology, Gaithersburg, Maryland, 20899-6102, USA. E-mail: gsrini@seas.upenn.edu; taner@seas.upenn.edu; Fax: +1-301-921-9847; Tel: +1-301-975-6228
[b]Department of Materials Science and Engineering, University of Pennsylvania, Philadelphia, Pennsylvania, 19104-6272, USA

† Electronic supplementary information (ESI) available: Additional, detailed XRD patterns, TG plots, FTIR spectra, and gas sorption isotherms of materials studied. See DOI: 10.1039/c1jm11699a

moieties.[22–24] In our very recent work, we successfully synthesized a first porous graphene oxide framework (GOF) material based on diboronic acid pillared GO layers.[6] Here we report the detailed synthesis of other porous GOFs from pillaring the GO layers with various linear boronic acids. The boronic acids that we used and our target GOF structures are schematically shown in Fig. 1. As we show below, the underlying strong boronate-ester bond formation between GO layers leads to improved stability over GO and much enhanced porosity after evacuation, storing twice the hydrogen at low pressures with respect to their surface areas than typical porous carbon materials. GOFs reveal that the accessible surface area and framework stability is strongly dependent on the type and length of cross-linker used as well as synthesis temperature.

2. Experimental details

Materials and synthesis

The detailed synthesis of GO is reported in our earlier work.[6] The GOF-L (L = 1PBA, 14PDBA, 4BPBA, 44BPDBA) materials are obtained by solvothermal synthesis at various temperatures between 80 °C to 150 °C for 48 h in methanol from equal amounts of GO and boronic acids, by mass: 1-phenylboronic acid (1PBA, Sigma Aldrich, ≥97%[25]), 1,4-phenyldiboronic acid (14PDBA, Alfa Aesar, 96%), 4-biphenylboronic acid (4BPBA, Tokyo Chemical Industry America), and 4,4'-biphenyldiboronic acid (44BPDBA, Alfa Aesar, 97%), respectively. The GO-control is obtained using the same solvothermal conditions without the boronic acid. The reduced GO (rGO) is obtained by solvothermal reduction of GO in methanol at 150 °C for 24 h and then used to synthesize rGOF-14PDBA by solvothermal method at 100 °C from the equal amounts by weight of reduced GO and 14PDBA. The products after solvothermal process are isolated by centrifugation and washed with methanol several times to remove any unreacted starting materials, and dried at room temperature prior to the characterization.

Characterization

X-ray diffraction (XRD) measurements are conducted on powder samples using a Rigaku X-ray diffractometer with Cu-Kα radiation. Fourier transform infrared (FTIR) spectroscopy is carried out using the KBr-pellet method in transmission mode on a NEXUS 670 FT-IR spectrometer. The spectrum was generated and collected 128 times and corrected for the background noise. The Raman spectra are obtained using 514 nm laser excitation on a LabRAM HR-VIS microRaman system. The thermogravimetry (TG) measurements are carried out on a TA instruments Q600 simultaneous DSC/TGA at a ramping rate of 2 °C min^{-1} under N_2 atmosphere. The N_2 sorption BET (Brunauer-Emmett-Teller) surface area measurements are performed on a Quantachrome Autosorb 1-C at 77 K. The high-pressure H_2 sorption at various temperatures is obtained using a home-built Sievert's type apparatus.[26]

3. Experimental results

3.1 GOFs synthesized at 100 °C

In our study, we found that the synthesis temperature had a critical effect on the formation of framework structure. The best samples are obtained at temperatures near 100 °C solvothermal process. The frameworks with well-defined layer structure are identified with XRD patterns given in Fig. 2. The precursor GO shows a single diffraction (001) peak at 2θ of *ca.* 11.5°, corresponding to the *c*-axis interlayer distance (*d*-spacing) of 0.76 nm between randomly stacked GO layers. We note that in graphite, due to AB stacking ordering, the (001) reflection is not allowed. The GOF samples exhibit a much larger shift in the (001) peak position toward lower angles, indicating the one-dimensional expansion of the GO layers along its *c*-axis with an increased *d*-spacing as high as 1.14 nm. It is important to note that the samples exhibit only expanded layer structure (001 reflection) without any signs of GO reduction as happened in other graphene hybrid, porous materials obtained with other linkers such as organic diisocyanate cross-linking.[10] In addition,

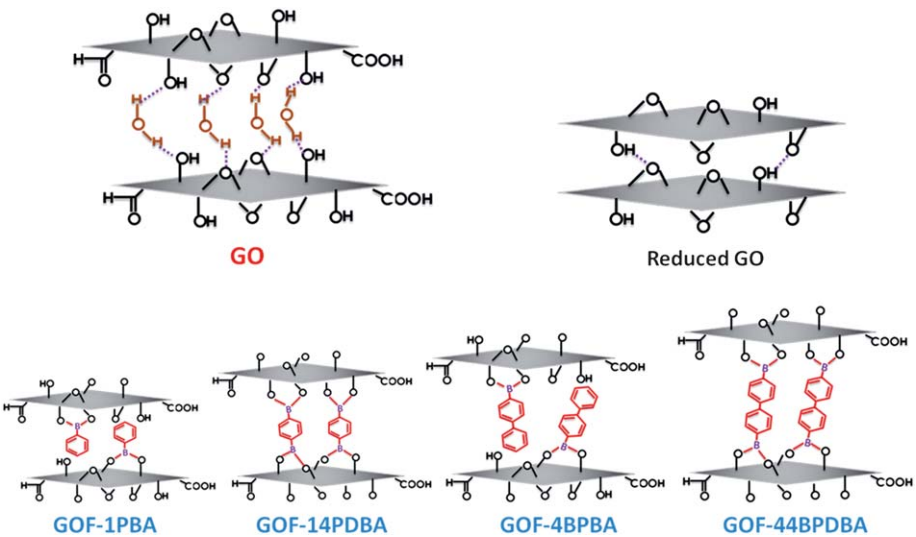

Fig. 1 Proposed GOF structures with various types of phenylboronate pillaring units.

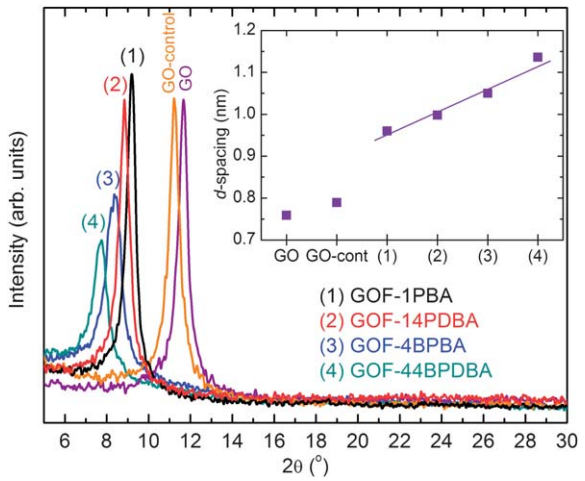

Fig. 2 XRD patterns of as-synthesized GOFs (at 100 °C solvothermal); Inset shows the variation of interlayer spacing with type and size of the pillaring unit.

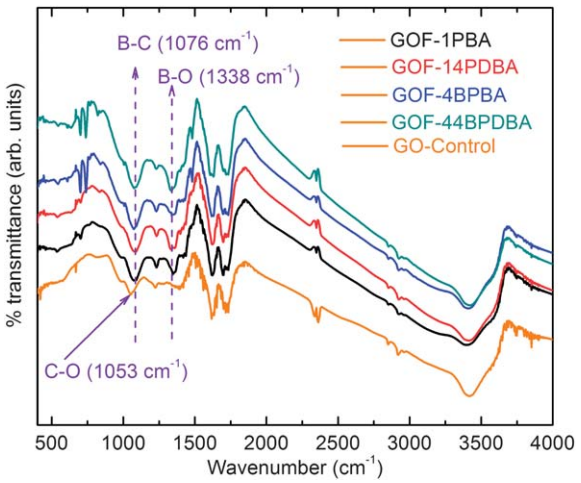

Fig. 3 FTIR spectra of as-synthesized GOFs (at 100 °C solvothermal).

the influence of different boronic acid pillaring units on *d*-spacing is shown in the inset to Fig. 2. As expected from the length of the pillaring unit, GOFs exhibit a gradual increase and well-defined *d*-spacing between GO layers with similarly good order, suggesting that the interlayer spacing is sensitive to the length of the pillaring unit. This strongly suggests that the pillaring units are not simply intercalated between GO layers parallel to the GO plane. If the boronic acids were situated parallel to the GO planes, we would not expect to see an increase in *d*-spacing with longer pillaring units as they all have the same width. Similarly if the pillaring units were exactly perpendicular to the GO layers, the *d*-spacing should not depend on the pillar concentration. Instead we observe that the *d*-spacing increases with pillar concentration, reaching the limit where the pillar units are perpendicular to the GO layers.[6] This strongly suggests that the pillaring units in our GOF samples are aligned randomly with some angle that is closer to being perpendicular with increasing pillar concentration. This makes sense as the pillar units have to find the right functional groups on both sides of GO surface to link them.

The functionality of the GO and pillaring mechanism, and thermal stability of framework structures are further characterized by FTIR, Raman scattering and TG analyses. Fig. 3 and S1† show the FTIR and Raman spectra of GOFs as well as the precursor GO. The IR spectrum of GO reveals characteristic vibrational bands corresponding to O–H stretching at 3300–3500 cm^{-1}, C=O stretching at ≈1720 cm^{-1}, C–OH stretching at ≈1244 cm^{-1}, and C–O stretching at ≈1053 cm^{-1}. The vibrations at ≈1380 and ≈1630 cm^{-1} correspond to O–H bending from hydroxyl/phenol groups and O–H vibration in water and are in good agreement with the literature.[1,2] However, GOFs show a clear, distinguishable additional IR mode at ≈1338 cm^{-1} corresponding to the B–O stretch due to cross-reaction of boronic acids with GO layers by boronate-ester formation.[23,24] In addition to the prominent B–C vibrations at ≈1076 cm^{-1}, the weaker IR modes in the low wavelength region <1000 nm in GOFs represents the presence of phenyl rings from the boronic acid pillaring units.[23,24] The Raman spectra (Fig. S1†) of GO and two different GOF samples are very similar and display two characteristic peaks of D-band at 1338 cm^{-1} and G-band at 1580 cm^{-1}, respectively. The D/G peak intensity ratio for GO and GOF samples are also very similar and close to one, suggesting that the surface functional groups in GO mostly remain and the main role of pillar units is to prop open the GO layers. Otherwise, the D peak intensity should decrease significantly if the GO surface functional groups were reduced during GOF formation.

The thermal stability of GOFs is analyzed using TG by heating under nitrogen atmosphere to 400 °C at a rate of 2 °C min^{-1} (Fig. 4). In agreement with previous reports, GO is thermally unstable and suffers rapid mass loss upon heating to about 200 °C. The initial step below 125 °C is associated with evaporation of trapped water molecules. The main mass loss (*ca.* 30%) between 150 °C to 200 °C is ascribed to the decomposition of oxygen containing functional groups to generate carbon dioxide and water. The plateau is seen above 220 °C with the total mass loss of 48%. Compared to GO, GOFs exhibit marked reduction in initial mass loss below 125 °C, and relatively higher structural stability by approximately 60 °C. It is worth to note that the decomposition temperature of the GOFs is also independent of

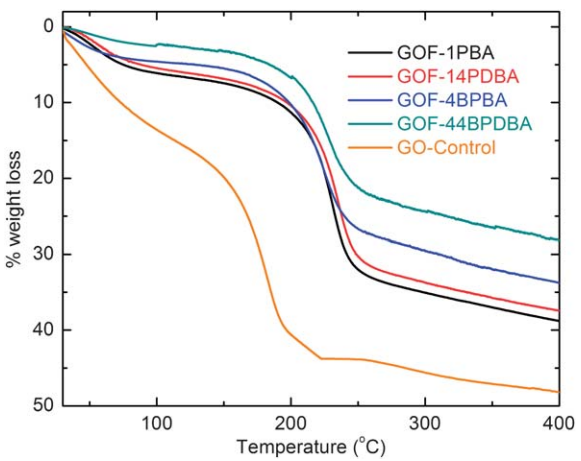

Fig. 4 TG analysis plots of as-synthesized GOFs (at 100 °C solvothermal).

constituent GO as well as boronic acids (Fig. S2†). The final mass loss of GOFs appears to be much lower than the GO, indicating the increased bulk between graphene layers due to the additional boron and carbons from pillared boronic acids and is consistent with the type and length of the phenylboronic acid pillaring unit.

To be useful for gas storage and/or separation, the GOFs must be permanently porous and stable after removal of trapped solvents. The retention of the expanded structure after evacuation to remove trapped molecules is further tested with powder XRD. Fig. S3† shows the XRD patterns and *d*-spacings of GO and GOF samples after evacuation at different temperatures. The samples evacuated at 120 °C retain their structural integrity, though with slightly decreased *d*-spacing that is attributed to the removal of adsorbed water/solvent molecules within the galleries.[27] Above 120 °C, there is a distinct difference between mono- and di-boronic acid pillared GOF structures. The mono-boronic acid derived GOF-L (L = 1PBA, 14PDBA, 4BPBA and 44BPBA) show much weaker intensity and smaller *d*-spacing after evacuation at 150 °C (inset to Fig. S3†).

It is clear from the TG and XRD structural analyses that the as-synthesized and room temperature dried samples contain water/solvent molecules within the pores. Therefore prior to the porosity and gas sorption analyses the samples were outgassed at 120 °C for 24 h. Fig. 5a and S4† represent the N_2 adsorption-desorption isotherms on precursor GO and GOFs. As observed previously,[6] the GO exhibits negligible surface area and porosity for gas sorption. In contrast, the expanded structure of GOFs exhibit reasonably larger accessible surface area for gas sorption. The samples subjected to the different outgassing temperatures (Fig. S4†) suggest that *ca.* 120 °C is the optimum outgassing temperature to produce the highest BET surface area. The isotherms of GOFs are invariably of Type I and indicate a microporous network. The surface area obtained by BET (Brunauer-Emmitt-Teller) method is about 470 $m^2 g^{-1}$ for GOF-14PDBA compared to *ca.* 10 $m^2 g^{-1}$ of GO, which explains the importance of pillaring GO sheets. The high pressure H_2 adsorption-desorption properties of all the GOFs at 77 K is shown in Fig. 5b, S4 and S5.† As expected, the H_2 isotherms of GOFs reveal similar trend in uptake that are more or less proportional to the BET surface areas. However, it is important to note that the obtained H_2 uptake capacities (1.2 to 0.4 wt%) are relatively high when compared to the other large number of porous materials known with respect to the generalized BET surface area.[28] For better understanding, we compare the H_2 adsorption capacity of our GOF samples against surface area with the other porous materials (Fig. 5c, dashed lines). It is well known that the maximum hydrogen uptake of all the classes of porous materials is linearly correlated to the apparent specific surface area. Typical activated carbon materials show a maximum H_2 uptake of *ca.* 1 wt% for every 500 $m^2 g^{-1}$ of specific surface area at 77 K and approximately 0.5 wt% for every 500 $m^2 g^{-1}$ at 1 atm and 77 K.[28,29] Per given surface area, the GOFs exhibit as much as twice the H_2 capacity at low pressures. Furthermore, GOFs also exhibit higher H_2 capacity when compared to the reduced graphenes in terms of given BET surface areas.[15,17,30] For instance, Ghosh *et al.*,[30] report 1.38 and 0.68 wt% of H_2 for the given BETs of 925 and 520 $m^2 g^{-1}$ respectively and Srinivas *et al.*,[15] obtained about 0.6 wt% of H_2

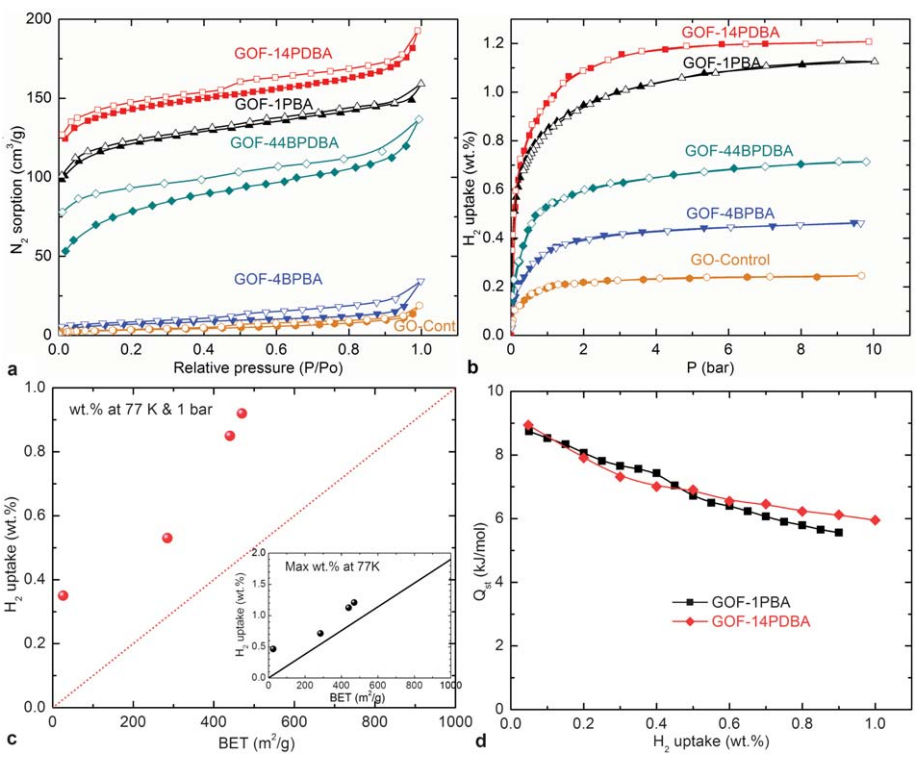

Fig. 5 a) N_2 adsorption-desorption isotherms, b) H_2 adsorption-desorption isotherms. c) Comparison of H_2 uptake with respect to the BET surface area of GOFs with generalized trend of porous materials,[28] and d) Isosteric heat of adsorption (Q_{st}) of GOF-1PBA and GOF-14PDBA[6] as a function of the amount adsorbed. All the GOFs synthesized at 100 °C and outgassed at 120 °C before gas sorption analysis.

for the BET of 640 $m^2 g^{-1}$, each at 77 K and 1 bar. It is worth to note that not all pillaring units are effective at increasing either the N_2 accessible surface area or hydrogen sorption. For example, despite the more interlayer spacing in GOF-4BPBA and GOF-44BPDBA, we observe largely decreased BET surface area when compared to the GOF-1PBA and GOF-14PDBA. In principle, the more expanded structure should exhibit more accessible surface area and gas sorption. However the observed trend here is directly correlated to the filling of the GO layers with the biphenyl-rings in agreement with TG results, thereby reducing the size and surface area of the pores for gas sorption.

To understand the sharp rise in H_2 uptake at very low pressures we further analyzed the gas adsorption at various temperatures (Fig. S5†) and calculated the uptake dependence of the heat of adsorption (Q_{st}) (Fig. 5d). Interestingly the obtained Q_{st} is twice as large as typical carbon nanostructures[15,28,31] and reduced graphenes (4–6 kJ mol^{-1}[15] and 1–3 kJ mol^{-1}[17]) and compares well with metal–organic frameworks materials with open metal centers.[28] This enhanced Q_{st} is probably due to optimum interlayer distance between GO layers in our samples where hydrogen molecules enter the interlayer spacing and then equally interacts with both graphene surface (*i.e.* slit-like pore), therefore doubling the binding energy. We note that the van der Waals (vdW) diameter of H_2 molecule is around 3 Å and the *d*-spacing in bare GO is 7.5 Å. Hence the optimum *d*-spacing is 10.5 Å, which is about what we observe for our GOF samples. If the *d*-spacing is larger than this value, the H_2 molecule between GO layers would be adsorbed on one of the GO surface and cannot interact effectively with the other side of the slit-like pore. In addition to the optimum *d*-spacing, the interaction between H_2 molecules and pillar units may also contribute significantly to the observed large Q_{st}. More studies, such as first-principles total-energy calculations, are needed to resolve the contribution from GO layers and the diboronic acid linkers to the total Q_{st}.

3.2 Effect of synthesis temperature

It has been shown that the GO is easily reduced by solvothermal methods,[32,33] indicating that temperature plays an important role in successful syntheses (Fig. 6). Keeping this in mind, we further tested the structure and porosity of GOF-1PBA and GOF-14PDBA obtained at various solvothermal synthesis temperatures. Fig. 6 represents the XRD patterns of GO, GOF-1PBA and GOF-14PDBA synthesized at different solvothermal temperatures. It clearly shows that the optimum temperature to obtain well-defined GOFs is around 100 °C. A further increase in the synthesis temperature above 100 °C, leads to a gradual disappearance of (001) peak and development of the characteristic (002) graphitic peak in agreement with the reduced GO.[32,33] In addition, the GOFs obtained at temperatures above 100 °C in solvothermal processes also exhibit a pronounced loss of BET surface area and thereby reduced H_2 uptake capacity (Fig. S6†) due to considerably decreased interlayer space as well as extent of B–O bond formation, as opposed to pillaring, of GO layers with boronic acids.

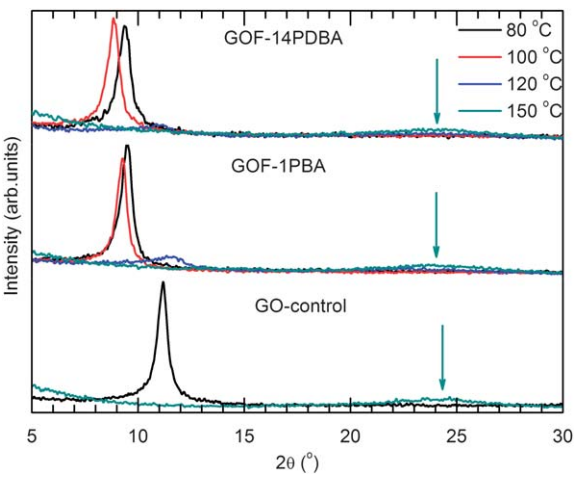

Fig. 6 XRD patterns of as-synthesized (room temperature dried) GO, GOF-1PBA and GOF-14PDBA obtained at different temperatures of solvothermal process.

4. Discussion

As revealed from XRD, FTIR, Raman, TG and gas sorption measurements, significant increase in interlayer graphene separation, modification in surface functional groups, increased thermal stability, and highly enhanced BET surface area as well as H_2 storage in the GOFs compared to that of precursor GO clearly suggests that the boronic acids act as pillaring units between adjacent GO layers by forming strong boronate-ester bonding. From the XRD-results, it is worthy to note that the increase in *d*-spacing with length of boronic acid is also an indication that the GO layers have been pillared by the boronic acid rather than merely intercalated by the planar phenyl-rings which would lie parallel to the graphene surfaces. Accordingly, the extensive data that we have support proposed GOF structures (see Fig. 1). The as-prepared GO contains significant amounts of water within the interlayer gallery as observed from the varying interlayer spacing depending on the hydration level (Fig. 6, S3 and S7[1,2,4,27,32]).† The water molecules play a critical role in mediating the interactions between adjacent GO layers most likely *via* a hydrogen-bonding network formed between epoxide (hydrogen-bond acceptor) and hydroxyl (both hydrogen-bond acceptor and donor) groups on the GO surfaces (Fig. 1). During the solvothermal synthesis, the interlayer water molecules are exchanged by methanol solvent molecules, which further expand the interlayer spacing, allowing the boronic acids to enter the interlayer space to react with OH functional group on the graphene surface. When the solvothermal temperature is increased well above 100 °C, we start to remove surface functional groups on GO, which reduces the interlayer distance significantly and suppresses the GOF formation. For instance, Fig. S7, S8† show that the framework structures did not occur in reduced/anhydrous stacked GO layers, *i.e.*, rGOF-14PDBA which was synthesized from reduced GO and 14PDBA by similar solvothermal method at 100 °C. Similarly, we did not get any framework structure if the synthesis temperature is near or above a 150 °C. The absence of framework structure in reduced GO is consistent with our hypothesis that we need surface functional groups in order to link the boronic acids on the surface of GO. This is also further supported by FTIR spectra (Fig. S8†), where all the GOF samples; GOF-1PBA and GOF–14PDBA synthesized at 150 °C and rGOF-14PDBA exhibit spectra similar to that of reduced GO without any signs of characteristic boronate-

ester B–O bonds or phenyl ring substitution B–C vibration bands. Apart from this, gas sorption results of GOFs obtained from the >100 °C solvothermal method (Fig. 6, S6†) clearly suggest that the reduction in interlayer space as well as degree of extensive boronate-ester bond formation show a marked effect in obtaining high accessible BET surface areas and H_2 uptake.

5. Conclusion

We demonstrated the successful solvothermal synthesis of porous graphene oxide frameworks by pillaring the graphene oxide sheets with linear boronic acids. As demonstrated from the XRD, the GOF structures are created with a marked increase in interlayer spacing of GO layers. The successful pillaring of boronic acids is further supported by FTIR where the evidence of boronate-ester bonding formation is clearly observed. The frameworks exhibit reasonably higher surface area about 470 $m^2 g^{-1}$ compared to the *ca.* 10 $m^2 g^{-1}$ for GO. The higher H_2 uptake for the given BET value is accounted for by their superior heat of adsorption compared to most of the other carbon-based porous sorbents. The optimum conditions to obtain well-defined interlayer space and maximum BET surface area is 100 °C solvothermal temperature and with 14PDBA linker. We found that the porous framework interlayer spacing, BET surface area and gas sorption is highly dependent on the synthesis temperature as well as length of the pillaring unit. There have been many theoretical studies that predict increase in hydrogen uptake of porous carbons due to increase in interlayer distance of graphite. However there are few successful experimental studies that report reasonable gas storage by pillaring the graphene planes using surface functionalization or well-known intercalation process. This is likely due to the filling up of the graphene interlayer space with guest molecules that leave little room for gas storage. However with our approach, it seems that it is possible to expand the GO layers with boronic pillar molecules while still keeping some available room for hydrogen adsorption. Finally, we note that based on our previous theoretical calculations,[6] the ideal GOF structures should have much higher surface area than what we have achieved thus far, suggesting we still have many functional groups and/or solvent molecules trapped in our samples. Hence, our next challenge is to remove these unreacted and/or trapped solvent molecules in our GOF samples to optimize the hydrogen uptake. Different activation procedures other than heat treatment, such as chemical reduction, to remove unreacted functional groups could improve the surface area and adsorption capacity of GOFs significantly. We are currently carrying out more detailed research along these lines. We hope that our results reported here will be valuable in searching new nanoporous materials based on cheap and environmentally friendly GO as a building block.

Acknowledgements

This work was supported by DOE BES Grant No. DE-FG02-08ER46522.

References

1 D. R. Dreyer, S. Park, C. W. Bielawski and R. S. Ruoff, The Chemistry of Graphene Oxide, *Chem. Soc. Rev.*, 2010, **39**, 228–240.
2 Y. Zhu, S. Murali, W. Cai, X. Li, J. W. Suk, J. R. Potts and R. S. Ruoff, Graphene and Graphene Oxide: Synthesis, Properties, and Applications, *Adv. Mater.*, 2010, **22**, 3906–3924.
3 H. Kim, A. A. Abdala and C. W. Macosko, Graphene/Polymer Nanocomposites, *Macromolecules*, 2010, **43**, 6515–6530.
4 K. W. Putz, O. C. Compton, M. J. Palmeri, S. T. Nguyen and L. C. Brinson, High-Nanofiller-Content Graphene Oxide–Polymer Nanocomposites *via* Vacuum-Assisted Self-Assembly, *Adv. Funct. Mater.*, 2010, **20**, 3322–3329.
5 D. R. Dreyer, H.-P. Jia and C. W. Bielawski, Graphene Oxide: A Convenient Carbocatalyst for Facilitating Oxidation and Hydration Reactions, *Angew. Chem. Int. Ed.*, 2010, **49**, 6813–6816.
6 J. Burress, S. Gadipelli, J. Ford, J. M. Simmons, W. Zhou and T. Yildirim, Graphene Oxide Framework Materials: Theoretical Predictions and Experimental Results, *Angew. Chem., Int. Ed.*, 2010, **49**, 8902–8904.
7 M. Fang, Z. Zhang, J. Li, H. Zhang, H. Lu and Y. Yang, Constructing Hierarchically Structured Interphases for Strong and Tough Epoxy Nanocomposites by Amine-rich Graphene Surfaces, *J. Mater. Chem.*, 2010, **20**, 9635.
8 S. Stankovich, D. A. Dikin, O. C. Compton, G. H. B. Dommett, R. S. Ruoff and S. T. Nguyen, Systematic Post-assembly Modification of Graphene Oxide Paper with Primary Alkylamines, *Chem. Mater.*, 2010, **22**, 4153–4157.
9 Y. Zhu, A. L. Higginbotham and J. M. Tour, Covalent Functionalization of Surfactant-Wrapped Graphene Nanoribbons, *Chem. Mater.*, 2009, **21**, 5284–5291.
10 D.-D. Zhang, S.-Z. Zu and B.-H. Han, Inorganic–Organic Hybrid Porous Materials based on Graphite Oxide Sheets, *Carbon*, 2009, **47**, 2993–3000.
11 A. B. Bourlinos, D. Gournis, D. Petridis, T. Szabó, A. Szeri and I. Dékány, Graphite Oxide: Chemical Reduction to Graphite and Surface Modification with Primary Aliphatic Amines and Amino Acids, *Langmuir*, 2003, **19**, 6050–6055.
12 M. Herrera-Alonso, A. A. Abdala, M. J. McAllister, I. A. Aksay and R. K. Prud'homme, Intercalation and Stitching of Graphite Oxide with Diaminoalkanes, *Langmuir*, 2007, **23**, 10644–10649.
13 M. Fang, K. Wang, H. Lu, Y. Yanga and S. Nutt, Single-layer Graphene Nanosheets with Controlled Grafting of Polymer Chains, *J. Mater. Chem.*, 2010, **20**, 1982–1992.
14 H. J. Salavagione, M. A. Gómez and G. Martínez, Polymeric Modification of Graphene through Esterification of Graphite Oxide and Poly(vinyl alcohol), *Macromolecules*, 2009, **42**, 6331–6334.
15 G. Srinivas, Y. Zhu, R. Piner, N. Skipper, M. Ellerby and R. Ruoff, Synthesis of Graphene-like Nanosheets and their Hydrogen Adsorption Capacity, *Carbon*, 2010, **48**, 630–635.
16 D. Long, W. Li, L. Ling, J. Miyawaki, I. Mochida and S.-H. Yoon, Preparation of Nitrogen-Doped Graphene Sheets by a Combined Chemical and Hydrothermal Reduction of Graphene Oxide, *Langmuir*, 2010, **26**, 16096–16102.
17 L. P. Ma, Z. S. Wu, J. Li, E. D. Wu, W. C. Ren and H. M. Cheng, Hydrogen Adsorption Behavior of Graphene Above Critical Temperature, *Int. J. Hydrogen Energy*, 2009, **34**, 2329–2332.
18 D. Zhou and B.-H. Han, Graphene-Based Nanoporous Materials Assembled by Mediation of Polyoxometalate Nanoparticles, *Adv. Funct. Mater.*, 2010, **20**, 2717–2722.
19 Z.-L. Hu, M. Aizawa, Z.-M. Wang, N. Yoshizawa and H. Hatori, Synthesis and Characteristics of Graphene Oxide-Derived Carbon Nanosheet-Pd Nanosized Particle Composites, *Langmuir*, 2010, **26**, 6681–6688.
20 A. D. Leonard, J. L. Hudson, H. Fan, R. Booker, L. J. Simpson, K. J. O'Neill, P. A. Parilla, M. J. Heben, M. Pasquali, C. Kittrell and J. M. Tour, Nanoengineered Carbon Scaffolds for Hydrogen Storage, *J. Am. Chem. Soc.*, 2009, **131**, 723–728.
21 G. K. Dimitrakakis, E. Tylianakis and G. E. Froudakis, Pillared Graphene: A New 3-D Network Nanostructure for Enhanced Hydrogen Storage, *Nano Lett.*, 2008, **8**, 3166–3170.
22 K. Severin, Boronic Acids as Building Blocks for Molecular Nanostructures and Polymeric Materials, *Dalton Trans.*, 2009, 5254–5264.
23 A. P. Côté, A. I. Benin, N. W. Ockwig, M. ÓKeeffe, A. J. Matzger and O. M. Yaghi, Porous, Crystalline, Covalent Organic Frameworks, *Science*, 2005, **310**, 1166–1170.
24 B. M. Rambo and J. J. Lavigne, Defining Self-Assembling Linear Oligo(dioxaborole)s, *Chem. Mater.*, 2007, **19**, 3732–3739.

25 Certain trade names and company products are mentioned in this paper to adequately specify the experimental procedure and equipment used. In no case does this imply recommendation or endorsement by NIST, nor does it imply that the products are necessarily the best available for this purpose.
26 W. Zhou, H. Wu, M. R. Hartman and T. Yildirim, Hydrogen and Methane Adsorption in Metal–Organic Frameworks: A High-Pressure Volumetric Study, *J. Phys. Chem. C*, 2007, **111**, 16131–16137.
27 F. Barroso-Bujans, S. Cerveny, A. Alegría and J. Colmenero, Sorption and Desorption Behavior of Water and Organic Solvents from Graphite Oxide, *Carbon*, 2010, **48**, 3277–3286.
28 K. M. Thomas, Adsorption and Desorption of Hydrogen on Metal–Organic Framework Materials for Storage Applications: Comparison with Other Nanoporous Materials, *Dalton Trans.*, 2009, 1487–1505.
29 J. Burress, M. Kraus, M. Beckner, R. Cepel, G. Suppes, C. Wexler and P. Pfeifer, Hydrogen storage in engineered carbon nanospaces, *Nanotechnology*, 2009, **20**, 204026.
30 A. Ghosh, K. S. Subrahmanyam, K. S. Krishna, S. Datta, A. Govindaraj, S. K. Pati and C. N. R. Rao, Uptake of H_2 and CO_2 by Graphene, *J. Phys. Chem. C*, 2008, **112**, 15704–15707.
31 M. Rubes and O. Bludsky, DFT/CCSD(T) Investigation of the Interaction of Molecular Hydrogen with Carbon Nanostructures, *ChemPhysChem*, 2009, **10**, 1868–73.
32 H. Wang, J. T. Robinson, X. Li and H. Dai, Solvothermal Reduction of Chemically Exfoliated Graphene Sheets, *J. Am. Chem. Soc.*, 2009, **131**, 9910–9911.
33 C. Nethravathi and M. Rajamathi, Chemically Modified Graphene Sheets Produced by the Solvothermal Reduction of Colloidal Dispersions of Graphite Oxide, *Carbon*, 2008, **46**, 1994–1998.